Noah G. Weiss
Paul V. Jones
Prasun Mahanti
Kang P. Chen
Thomas J. Taylor
Mark A. Hayes

Department of Chemistry and Biochemistry, Arizona State University, USA

Received January 14, 2011
Revised March 9, 2011
Accepted March 10, 2011

Research Article

Dielectrophoretic mobility determination in DC insulator-based dielectrophoresis

Insulator-based dielectrophoresis (iDEP) is a powerful tool for separating and characterizing particles, yet it is limited by a lack of quantitative characterizations. Here, this limitation is addressed by employing a method capable of quantifying the DEP mobility of particles. Using streak-based velocimetry the particle properties are deduced from their motion in a microfluidic channel with a constant electric field gradient. From this approach, the DEP mobility of 1 μm polystyrene particles was found to be $-2 \pm 0.4\ 10^{-8}\,\mathrm{cm}^4/(\mathrm{V}^2\,\mathrm{s})$. In the future, such quantitative treatment will allow for the elucidation of unique insights and rational design of devices.

Keywords:
Dielectrophoresis / Dielectrophoretic mobility / Velocimetry
DOI 10.1002/elps.201100034

1 Introduction

Particles are ubiquitous in our bodies and our environment. This class of materials includes cells, organelles, nanoparticles, aerosols, large proteins and DNA strands, bacteria, and viruses – among other organic and inorganic debris. Dielectrophoresis (DEP) has emerged as an important technique for manipulating micro- to nano-scale particles [1, 2]. The nature of this force, described over 50 years ago by Pohl, depends on a particle's polarizability in a non-uniform electric field (Eq. 1) [3]. The DEP force experienced by a spherical particle is described as follows:

$$F = 4\pi\varepsilon_f r_p^3 \mathrm{Re}(f_{cm})(E\cdot\nabla)E = 2\pi\varepsilon_f r_p^3 \mathrm{Re}(\nu)\nabla E^2$$
$$\mathrm{Re}(f_{cm}) = \frac{\sigma_p - \sigma_f}{\sigma_p + 2\sigma_f} \quad f < 100\,\mathrm{kHz} \qquad (1)$$

where ε_f is the permittivity of the fluid, r_p is the particle radius, $\mathrm{Re}(f_{cm})$ is the real part of the Clausius–Mossoti factor defined by the particle and fluid conductivities (σ) at low frequency (f), and E is the electric field. At higher frequencies the conductivities are replaced by frequency-dependent permittivities. According to this relationship, to have a DEP force on a non-charge-containing species there must be a non-uniform field and a particle that has a different conductivity/permittivity relative to the fluid.

It is important to note that DEP can be operated in AC or DC modes using either shaped conductors or using insulators to generate field gradients [4]. The emphasis in this work is on DC insulator-based dielectrophoresis (DC iDEP). The initial and most popular design for DC iDEP is a microfluidic channel employing an array of insulating structures (Fig. 1A) [5–19]. Channels with obstructions (Fig. 1B) [20–26], serpentine features [27, 28], and converging–diverging or saw-tooth features (Fig. 1C) [29–33] have also been established in DC iDEP. Similar iDEP designs employ AC fields (10 Hz–10 MHz) to gain additional DEP control through frequency modulation of the Clausius–Mossoti factor [34–38]. Additionally, a contactless AC iDEP approach where the sample is completely isolated from the electrodes has been shown [39, 40]. In all of the designs an insulating material (e.g. glass, polymer, etc.) is used to create regions where the electric field is constricted to generate a field gradient and a DEP force. These devices deflect, stream, or trap particles in a composition-dependent manner for separation or concentration.

While Eq. (1) is widely accepted, it is usually only considered qualitatively when considering actual experimental data. Most discussions of real data rarely advance beyond an analysis of positive (toward stronger fields) versus negative (toward weaker fields) DEP. This is somewhat odd since there is extensive quantitative theory and modeling of DEP [31–34, 41, 42]. One detailed study did indicate some unique deviations from Eq. (1) from ionic effects [43]. DEP techniques are growing in popularity and with this interest it becomes increasingly important to develop detailed and quantitative metrics for the field.

It is often unreasonable to accurately calculate the DEP force that is exerted on a particle from first principles and this provides, perhaps, one explanation for the relative paucity of quantitative application of theory to experimental data. The difficulty arises from the uncertainties in the permittivity, particle size/shape, deformability, and local field gradients. Furthermore, Eq. (1) assumes a spherical particle having a permanent or induced dipole and fails to describe complex shapes or multipolar states [44].

Correspondence: Professor Mark Hayes, Department of Chemistry and Biochemistry, PO Box 871604, Tempe, AZ 85287-1604, USA
E-mail: mhayes@asu.edu
Fax: +1-480-965-2747

Abbreviations: DEP, dielectrophoresis; **iDEP,** insulator-based dielectrophoresis

Colour Online: See the article online to view Figs. 2 and 3 in colour.

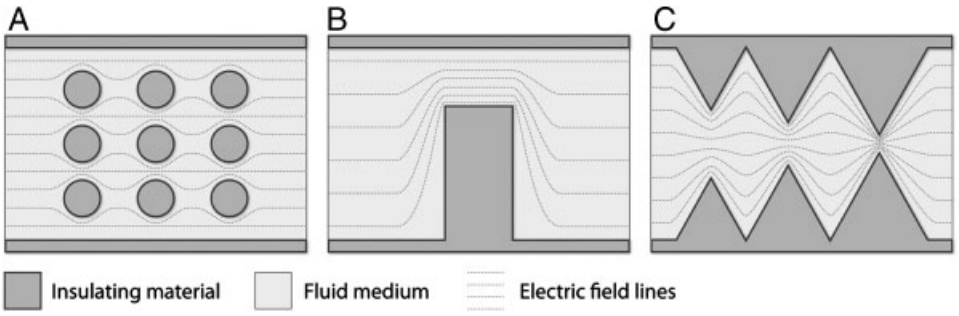

Figure 1. Schematic illustrations of the most common types of iDEP devices where the insulating material (dark gray) penetrates the fluid medium (light gray) and pinches the electric field lines (dashed lines). Examples shown include the (A) array of insulators [5–19, 35–38], (B) obstructed channel [20–26, 34], and (C) converging-diverging or saw-tooth [29–33].

A practical solution to determining the DEP properties of particles is to experimentally determine the relative DEP velocity in a known gradient. This is analogous to the electrophoretic or electroosmotic mobility that is routinely measured in electrophoresis with a known electric field. Previously, methodologies have been developed for measuring a DEP mobility in AC-DEP [43, 45–47]. Although useful for AC applications, these approaches are limited because they define the DEP mobility parameter to be dependent on the device-specific electric field properties (device parameters actually appear in the definitions of the mobility). Thus, the mobility constants are specific to the particular device geometries used and cannot be ported to iDEP systems. To quantify DEP effects from the complex geometries of current iDEP designs (Fig. 1A and C) and allow detailed investigations resulting in accurate models, a universal quantitative metric of the DEP particle properties is needed. Moreover, if the DEP properties are known the electric field profile necessary for a particular outcome can be determined. With the aid of modeling software, iDEP systems can be rationally designed to generate the necessary electric field to target specific analytes (e.g. bacteria or virus).

In this work, we initiate a strategy to quantitatively determine DEP properties of particles in iDEP settings by defining the DEP mobility and demonstrating an approach to measure it in a converging microfluidic channel. This method relies on streak-based velocimetry to generate the spatial velocity profile of particles. From this the DEP and electrokinetic mobilities of polystyrene particles are simultaneously determined.

2 Materials and methods

2.1 Device fabrication

A microfluidic channel was fabricated using standard soft lithography using the elastomer PDMS from a Slygard 184 kit (Dow/Corning, Midland, MI, USA). PDMS was cast over a master wafer that contained an AZ 4620 photoresist pattern (AZ Electronic Materials, Branchburg, NJ, USA) to create channel impressions. The resist thickness was characterized with a Tencor P2 Profilometer and found to have a depth of 10 μm. After casting the PDMS over the master wafer it was cured at 70°C for 1 h and subsequently access holes were punched. An oxygen plasma was used to render the channels hydrophilic and generate a self-sealing surface. Finally, a clean glass microscope slide was used as a cover plate to enclose the microfluidic PDMS channel.

2.2 DEP experiments

The microfluidic channel was initially filled with buffer solution and allowed to equilibrate at rest for 10 min. The buffer consisted of 5 mM aspartic acid pH 3.1 and had a conductivity of 250 μS/cm or specific resistivity of 4000 Ω cm (Sigma Aldrich, St. Louis, MO, USA). Solution conductivities were measured using an Orion 3 Star conductivity meter (Thermo Fischer, Walthan, MA, USA). Sulfated polystyrene particles 1 μm in size and fluorescently labeled (Invitrogen, Carlsbad, CA, USA) were diluted to a concentration of approximately 5×10^6 particles/mL in the working buffer and sonicated for 15 min. Particles were introduced into the device using hydrostatic pressure initiated by a height difference in the two reservoirs. At the start of an experiment the pressure was equilibrated to stop hydrodynamic flow, and then 1500 V was applied from a Bertran Series 225 power supply (Bertran, Brooklyn, NY, USA) using two platinum electrodes dipped into the reservoirs with anode in region 1 and cathode in region 3. Particle motion was imaged using an Osram mercury short arc H30 103 w/2 light source and a 4 × objective on an inverted microscope (Olympus, Center Valley, PA, USA). Movies were collected using a QICAM CCD camera (Q Imaging, Surrey, British Columbia, Canada) and Streampix III software (Norpix, Montreal, Quebec, Canada). Depending on the experiment, the field of view was approximately 1.6 × 1.2 mm in region 1 or 2 (Fig. 2A) and the exposure time was adjusted to 30, 60, or 90 ms corresponding to 19.1, 16.6, or 11.1 frames per second, respectively.

2.3 Velocimetry analysis and data analysis

The velocity data are automatically generated from the streaked particle images using an algorithm. The details of

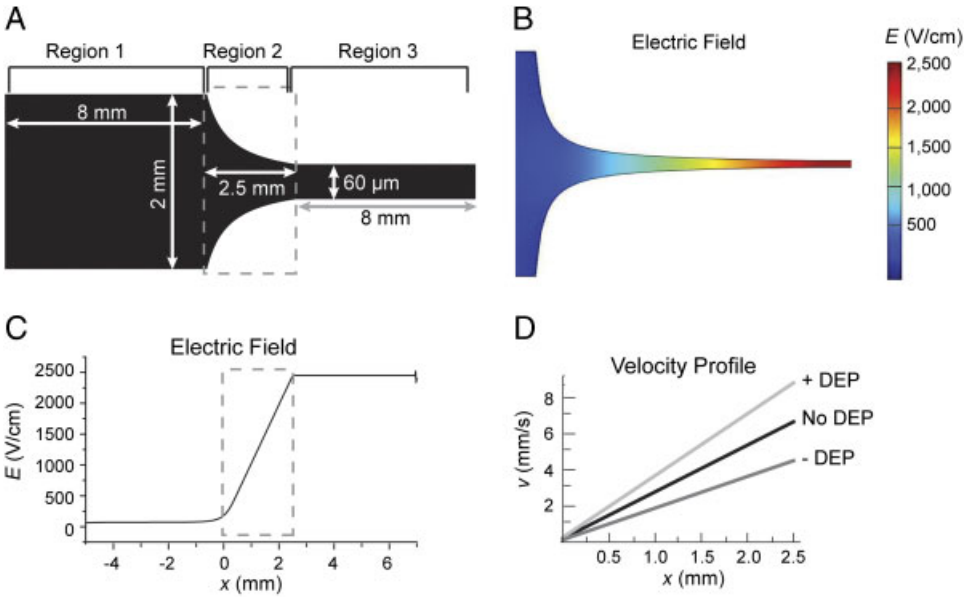

Figure 2. (A) Diagram and dimensions of iDEP device used consisting of wide uniform segment (region 1), taper segment (region 2), and narrow uniform segment (region 3). (B and C) COMSOL simulation of electric field of iDEP device. Dashed box indicates region 2. (D) Theoretical velocity profile in region 2 based on Eq. (9) in the case of positive, zero, or negative DEP using hypothetical mobility and electric field values.

the method have been described elsewhere but the main steps are briefly described here (P. Mahanti et al., manuscript in preparation; http://www.public.asu.edu/~mhayes/). Frames captured during the imaging process serve as the algorithm input. A 20 pixel strip is cropped from the center of the image frame and the streaks are identified from the background by image thresholding. Velocities are estimated by dividing the streak length, identified as the distance between the starting and ending points of a streak, by the exposure time. These velocities are then spatio-temporally averaged over the entire cropped region to generate the centerline velocity.

Manual tracking of particles was done using the ImageJ software (http://rsbweb.nih.gov/ij/). The image stack was cropped to a region 20 pixels wide along the channel centerline. The brightness and contrast was increased to allow for better visualization of particles and streaked images. The x coordinates of a single particle were tracked as it moved through the region of view by manually selecting the center of the particle's fluorescence. There was no problem with particles defocusing since the channel depth is on the order of 10 μm. Dilute particle concentrations and optimal camera conditions provided well resolved and continuous particle trajectories. Therefore, particles were confidently identified in consecutive frames manually without need for a nearest neighbor algorithm. For each experiment, at least 50 different particles were tracked in the same manner. The x-component particle velocity as it moved from x_a to x_b was assigned to the mean position of $x_a$and x_b and was calculated as follows:

$$v\left(\frac{x_a+x_b}{2}\right)_x = \frac{x_b - x_a}{\Delta t} \tag{2}$$

The elapsed time, Δt, between consecutive frames is the inverse of the frame rate (16.6 fps).

The mean velocity $<v_p>$ is determined from several hundred streak-based velocity measurements from a single 90 ms exposure experiment within region 1 (Fig. 2A). The longer exposure time produced particle streak images allowing for streak velocity assessment. In region 1 the electric field is uniform and the electrokinetic mobility (μ_{EK}) is calculated using the following convention:

$$\mu_{EK} = (\mu_{EO}+\mu_{EM}) = \frac{\langle v_{p,x}\rangle}{E} \tag{3}$$

where μ_{EM} is the electrophoretic mobility and μ_{EO} is the electroosmotic mobility. A linear best fit was obtained from the velocimetry data in region 2 (Figs. 2A, 3B, and 4A and B).

3 Results and discussion

3.1 Particle motion and device design

In contrast to works based on AC-DEP [43, 45–47], the DEP mobility (μ_{DEP}) is defined independent of the electric field and thus becomes a universal parameter, consistent with electrophoretic and electroosmotic mobilities, and follows the typical convention in iDEP (Eq. 4) [6, 7, 12, 13, 16, 17, 31, 40]. In other words this definition of DEP mobility is intrinsic to the particle and represents the relative DEP velocity per unit electric field gradient squared as shown

$$v_{DEP} = \mu_{DEP}\nabla E^2$$
$$\mu_{DEP} = \frac{\varepsilon_f r_p^2 \mathrm{Re}(f_{cm})}{3\eta} \tag{4}$$

where v_{DEP} is the DEP velocity and η is the fluid viscosity. Furthermore, an ideal method for quantifying iDEP ought to simultaneously quantify other electrokinetic effects (electroosmosis and electrophoresis). This is particularly important considering electroosmotic flow can vary by more than 10% [6]. A clear approach to quantifying the DEP velocity emerges by examining the equations of motion.

The motion of a spherical particle with negligible particle–particle interactions under the influence of a DC electric field in iDEP is extensively described by Chen et al. [31]. The velocity along the x direction ($v_{p,x}$), the axis of the applied current, is given by

$$v_{p,x} = E\left(\mu_{EO}+\mu_{EM}+\mu_{DEP}\frac{\partial E}{\partial s}\right)\cos\theta - \frac{\mu_{DEP}E^2}{R}\sin\theta \qquad (5)$$

where s is the arc length along the field line, θ is the angle between the tangent of the field line and the x-axis, and R is the radius of curvature of the field line. At the centerline of a symmetrical channel, the field lines are parallel to the x-axis. In other words $\theta = 0$ which simplifies Eq. (5) to

$$v_{p,x} = E\left(\mu_{EK}+\mu_{DEP}\frac{\partial E}{\partial x}\right) \qquad (6)$$

where the combined electrokinetic mobility is defined as $\mu_{EK} = \mu_{EO}+\mu_{EM}$. According to Eq. (6), μ_{DEP} can be calculated by measuring the x-component of the particle velocity along the channel centerline. Traditionally, positive μ_{EK} is defined as movement toward the negative electrode and positive μ_{DEP} is defined as movement toward high field strength. The same convention is followed here since the experiments are carried out with these two conditions aligned.

The microfluidic channel consists of a wide uniform area segment (region 1), a constricting taper segment (region 2), and a narrow uniform area segment (region 3) (Fig. 2A). The taper was designed to create a linearly increasing electric field, or a constant gradient, since this would generate the simplest DEP force (Eq. 6 and Fig. 2B and C). This is similar in design to a conductive polymer used for equilibrium gradient focusing [48]. Given a constant channel height (h) determined by the photoresist thickness, the channel cross-sectional area (A) varies inversely with x as

$$A(x) = h \times w_2(x) = h\frac{w_1}{(1+kx)} \quad 0 \le x \ge 2.5\,\text{mm} \qquad (7)$$

where w_2 is the channel width of region 2, the taper starts and ends at $x = 0$ and $x = 2.5$ mm, respectively, w_1 is the width of region 1, and k is the rate at which the channel tapers. The electric field is defined along the length of the channel ($E(x)$) is calculated by substituting Eq. (5) into the current density ($J(x)$) relation:

$$\begin{aligned} E(x) &= J(x)\rho \\ E(x) &= \gamma(1+kx) \quad \gamma = \frac{i\rho}{w_1 h} \quad 0 \le x \ge 2.5\,\text{mm} \end{aligned} \qquad (8)$$

Substituting Eq. (8) into Eq. (6) gives the velocity profile along the centerline ($v_{p,x}(x)$):

$$\begin{aligned} v_{p,x}(x) &= \gamma(1+kx)(\mu_{EK}+\gamma k\mu_{DEP}) \\ v_{p,x}(x) &= (\gamma^2 k^2\mu_{DEP}+\gamma k\mu_{EK})x+(\gamma^2 k\mu_{DEP}+\gamma\mu_{EK}) \end{aligned} \qquad (9)$$

Thus, particles experience a linear velocity increase as they move through the taper region. The slope of the velocity profile depends on both a DEP and electrokinetic term in Eq. (7). Therefore, according to this logic, the velocity slope will be steeper in the case of positive DEP and shallower in the case of negative DEP compared with that predicted if there is no DEP force (Fig. 2D). For these experiments $w_1 = 2$ mm, $k = 12.93\,\text{mm}^{-1}$, $h = 0.01$ mm, $\gamma = 8$ V/mm and the taper ended at $x = 2.5$ mm.

3.2 Streak-based velocimetry

One challenge in estimating particle velocities in iDEP devices is the wide range of velocities frequently encountered, which generate streaked particle images. For example, the spatial field gradients typically employed can create up to a 100-fold increase in the electroosmotic transport velocity. This led to the pursuit of a streak-based velocimetry approach rather than traditional micro-particle image velocimetry techniques [49].

Streak-based velocimetry operates by associating the length and trajectory of a streak in a blurred image with the exposure time to estimate the velocity field. As particles move from a weak to strong electric field they accelerate, and thus, the distance traveled in a single exposure becomes greater as observed by streak lengths in a captured image (Fig. 3A). An automated algorithm detects, processes, and determines the velocities traveled by the particles at all pixels across the image sequence. The particle velocity linearly increases along the x-axis and remains relatively constant along the y-axis (RSD 5%) within the depicted centerline strip (Fig. 3B). This is consistent with the expectation that the electric field is parallel to the x-axis (Eq. 6) and it linearly increases in magnitude (Eq. 8) within this region. The x-dimension has been cropped to exclude the beginning and ending portions of the taper where particles travel either too slow or fast for precise streak velocimetry assessment, respectively. Overall, Eq. (9) is considered to accurately describe the velocity profile. Furthermore, the constant

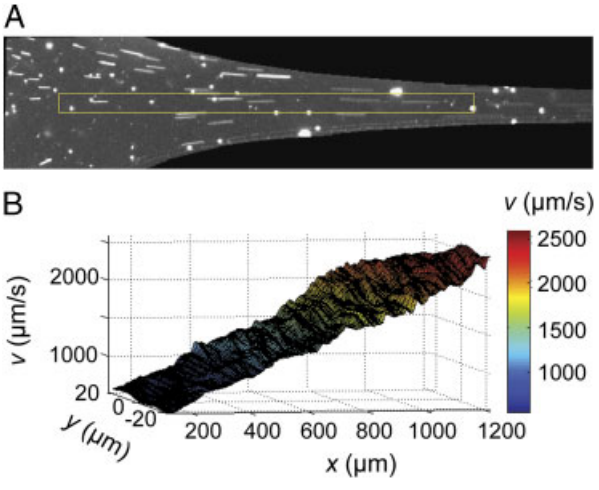

Figure 3. Streak velocimetry processing showing (A) an overlaid image sequence showing particle streak images and (B) the resultant spatial velocity estimation deduced from streak analysis. The region where data was analyzed and processed is highlighted by the light bounding box in (A).

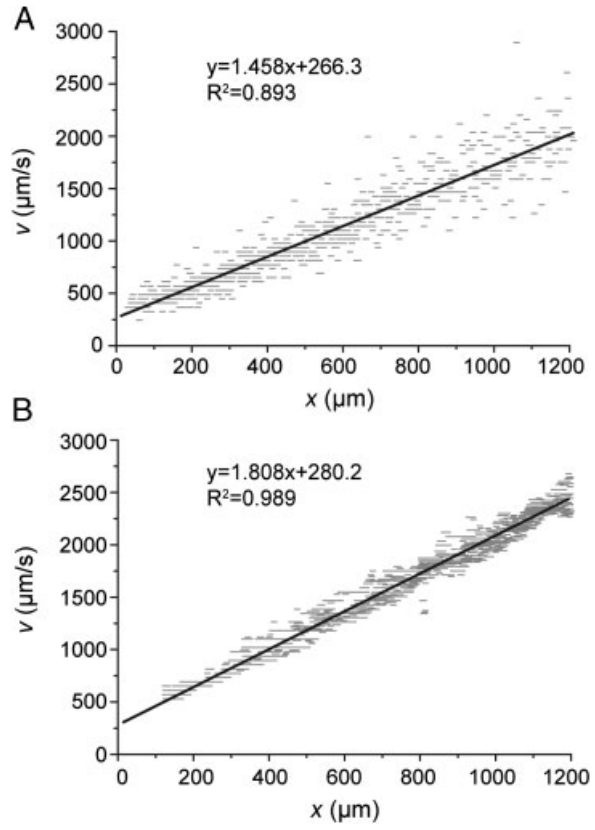

Figure 4. Comparison of velocimetry result between (A) manual particle tracking and (B) automated streak analysis (before averaging). In each case several hundred velocity estimations were made across the device and linear best fits were generated.

velocity along the *y*-axis allows spatiotemporal averaging to improve the centerline velocity estimation.

In addition to streak-based analysis, particle velocities were assessed using manual tracking for comparison. Clearly, the automated streak analysis is more precise compared with the manual particle tracking (Fig. 4A and B), and thus there is greater confidence in the slope determined by the streak analysis. This difference in precision is associated with the elongation of the imaged particles as they accelerate. Substantial uncertainty is introduced when manually tracking a particle's center of mass if the particle motion produces a streaked image. Automated streak tracking avoids this problem since it relies on the blurred streak images for velocity estimation.

3.3 Electrokinetic and DEP mobilities

As defined in Eq. (4), the DEP mobility describes a non-charge containing particle's polarizability in a particular fluid medium and primarily depends on a particle's size and Clausius–Mossoti factor. Thus, there will be a broad spectrum of DEP mobilities given the diversity of particle sizes, charges, and ionic properties. In fact the richness of this term suggests that within a single particle type there could be significant microheterogeneity to create sub-populations with unique mobility constants. Supporting this idea is the observation that charge properties of particles have been found to be much broader compared with molecules [50, 51].

The streak-based velocity estimations were used to calculate the system properties. Using 1 μm polystyrene particles the electrokinetic mobility was estimated to be $3.5 \times 10^{-4}\,cm^2/(V\,s)$ as calculated by Eq. (3) using the velocity data from region 1. This is considered a reasonable result and is likely dominated by electroosmotic flow considering its similarity to other electroosmotic mobility estimations [6, 52]. The DEP mobility of polystyrene particles was found to be $-2 \pm 0.4 \times 10^{-8}\,cm^4/(V^2\,s)$ from the slope in Eq. (9). The statistics are from three separate experiments that involved over 1000 velocity measurements each. This result agrees with the general finding that polymeric particles exhibit negative DEP under similar conditions [5, 8, 11]. Subtle variations in electroosmotic flow, particle heterogeneity, and variance in the velocity estimation likely contribute to the 20% RSD observed.

Under these particular conditions the electrokinetic velocity is about twice the magnitude of the DEP velocity based on calculations of the individual terms in Eq. (9). The relative DEP velocity could be increased by increasing the applied voltage, reducing electroosmotic flow, or utilizing steeper field gradients. However, particle motion rapidly changes direction in these regimes complicating velocity associations. For optimal quantitative analysis, the DEP motion must be observable but not predominant.

4 Concluding remarks

An approach to simultaneously quantifying the electrokinetic and DEP properties of particles in iDEP is discussed. Critical to the success of such analysis is the accurate and precise estimation of particle velocities. Presently, streak-based velocimetry was found to be more precise than manual particle tracking and has the advantage of automation. From this approach we determined polystyrene particles have a DEP mobility of $-2 \pm 0.4 \times 10^{-8}\,cm^4/(V^2\,s)$. In future studies mobility constants will be characterized under various conditions to construct a DEP profile of particular particle populations. Quantitative approaches like this one enable an unprecedented evaluation of iDEP and provide a metric for standardization. Ideally, discussions will eventually evolve from subjective descriptions of particle behaviors to more objective quantitative responses.

The authors acknowledge facilities and staff at the Center for Solid State Electronic Research (CSSER) for assistance with microfluidic fabrication. M. A. H. acknowledges support in part with NIH grants 2RO1EB004761-06 and R21EB010191-01A1.

The authors have declared no conflict of interest.

5 References

[1] Lapizco-Encinas, B. H., Rito-Palomares, M., *Electrophoresis* 2007, *28*, 4521–4538.

[2] Zhang, C., Khoshmanesh, K., Mitchell, A., Kalantar-zadeh, K., *Anal. Bioanal. Chem.* 2010, *396*, 401–420.

[3] Pohl, H. A., *J. Appl. Phys.* 1951, *22*, 869–871.

[4] Pethig, R., *Biomicrofluidics* 2010, *4*, 022811.

[5] Cummings, E. B., Singh, A. K., *Anal. Chem.* 2003, *75*, 4724–4731.

[6] Martinez-Lopez, J. I., Moncada-Hernandez, H., Baylon-Cardiel, J. L., Martinez-Chapa, S. O., Rito-Palomares, M., Lapizco-Encinas, B. H., *Anal. Bioanal. Chem.* 2009, *394*, 293–302.

[7] Kwon, J.-S., Maeng, J.-S., Chun, M.-S., Song, S., *Microfluid. Nanofluidics* 2008, *5*, 23–31.

[8] Lapizco-Encinas, B. H., Simmons, B. A., Cummings, E. B., Fintschenko, Y., *Anal. Chem.* 2004, *76*, 1571–1579.

[9] Baylon-Cardiel, J. L., Lapizco-Encinas, B. H., Reyes-Betanzo, C., Chavez-Santoscoy, A. V., Martinez-Chapa, S. O., *Lab Chip* 2009, *9*, 2896–2901.

[10] Mela, P., van den Berg, A., Fintschenko, Y., Cummings, E. B., Simmons, B. A., Kirby, B. J., *Electrophoresis* 2005, *26*, 1792–1799.

[11] Ozuna-Chacon, S., Lapizco-Encinas, B. H., Rito-Palomares, M., Martinez-Chapa, S. O., Reyes-Betanzo, C., *Electrophoresis* 2008, *29*, 3115–3122.

[12] Cummings, E. B., *IEEE Engineering in Medicine and Biology Magazine* 2003, *Nov/Dec*, 75–84.

[13] Lapizco-Encinas, B. H., Simmons, B. A., Cummings, E. B., Fintschenko, Y., *Electrophoresis* 2004, *25*, 1695–1704.

[14] Lapizco-Encinas, B. H., Davalos, R. V., Simmons, B. A., Cummings, E. B., Fintschenko,Y., *J. Microbiol. Methods* 2005, *62*, 317–326.

[15] Ozuna-Chacon, S., Lapizco-Encinas, B. H., Rito-Palomares, M., Collado-Arredondo, E., Martinez-Chapa, S. O., *Revista Mexicana De Ingenieria Quimica* 2007, *6*, 329–335.

[16] Lapizco-Encinas, B. H., Ozuna-Chacon, S., Rito-Palomares, M., *J. Chromatogr. A* 2008, *1206*, 45–51.

[17] Gallo-Villanueva, R. C., Rodriguez-Lopez, C. E., Diaz-de-la-Garza, R. I., Reyes-Betanzo, C., Lapizco-Encinas, B. H., *Electrophoresis* 2009, *30*, 4195–4205.

[18] Moncada-Hernandez, H., Lapizco-Encinas, B. H., *Anal. Bioanal. Chem.* 2010, *396*, 1805–1816.

[19] Davalos, R. V., McGraw, G. J., Wallow, T. I., Morales, A. M., Krafcik, K. L., Fintschenko, Y., Cummings, E. B., Simmons, B. A., *Anal. Bioanal. Chem.* 2008, *390*, 847–855.

[20] Hawkins, B. G., Smith, A. E., Syed, Y. A., Kirby, B. J., *Anal. Chem.* 2007, *79*, 7291–7300.

[21] Kang, Y., Li, D., Kalams, S. A., Eid, J. E., *Biomed. Microdevices* 2008, *10*, 243–249.

[22] Kang, K. H., Xuan, X., Kang, Y., Li, D., *J. Appl. Phys.* 2006, *99*, 064702.

[23] Kang, K. H., Kang, Y., Xuan, X., Li, D., *Electrophoresis* 2006, *27*, 694–702.

[24] Barrett, L. M., J, S. A., Singh, A. K., Cummings, E. B., Fiechtner, G. J., *Anal. Chem.* 2006, *77*, 6798–6804.

[25] Barbulovic-Nad, I., Xuan, X., Lee, J. S. H., Li, D., *Lab Chip* 2006, *6*, 274–279.

[26] Lewpiriyawong, N., Yang, C., Lam, Y. C., *Biomicrofluidics* 2008, *2*, 034105.

[27] Zhu, J., Tzeng, T.-R. J., Hu, G., Xuan, X., *Microfluid. Nanofluidics* 2009, *7*, 751–756.

[28] Church, C., Zhu, J., Nieto, J., Keten, G., Ibarra, E., Xuan, X., *J. Micromech. Microeng.* 2010, *20*, 065011.

[29] Pysher, M. D., Hayes, M. A., *Anal. Chem.* 2007, *79*, 4552–4557.

[30] Staton, S. J. R., Chen, K. P., Taylor, T. J., Pacheco, J. R., Hayes, M. A., *Electrophoresis* 2010, *31*, 3634–3641.

[31] Chen, K. P., Pacheco, J. R., Hayes, M. A., Staton, S. J. R., *Electrophoresis* 2009, *30*, 1441–1448.

[32] Ai, Y., Joo, S. W., Jiang, Y., Xuan, X., Qian, S., *Electrophoresis* 2009, *30*, 2499–2506.

[33] Ai, Y., Qian, S., Liu, S., Joo, S. W., *Biomicrofluidics* 2010, *4*, 013201.

[34] Kirby, B. J., Hawkins, B. G., *Electrophoresis* 2010, *31*, 3622–3633.

[35] Jen, C.-P., Huang, C.-T., Shih, H.-Y., *Microsyst. Technol.* 2010, *16*, 1097–1104.

[36] Ros, A., Hellmich, W., Regtmeier, J., Duong, T. T., Anselmetti, D., *Electrophoresis* 2006, *27*, 2651–2658.

[37] Regtmeier, J., Duong, T. T., Eichhom, R., Anselmetti, D., Ros, A., *Anal. Chem.* 2007, *79*, 3925–3932.

[38] Chou, C.-F., Tegenfeldt, J. O., Bakajin, O., Chan, S.S., Cox, E. C., Darnton, N., Duke, T., Austin, R. H., *Biophys. J.* 2002, *83*, 2170–2179.

[39] Shafiee, H., Sano,M. B., Henslee, E. A., Caldwell, J. L., Davalos, R. V., *Lab Chip* 2010, *10*, 438–445.

[40] Shafiee, H., Caldwell, J. L., Sano, M. B., Davalos, R. V., *Biomed. Microdevices* 2009, *11*, 997–1006.

[41] Winter, W. T., Welland, M. E., *J. Phys. D: Appl. Phys.* 2009, *42*, 045501.

[42] Ai, Y., Qian, S., *J. Colloid Interface Sci.* 2010, *346*, 448–454.

[43] Tsukahara, S., Sakamoto, T., Watarai, H., *Langmuir* 2000, *16*, 33866–33872.

[44] Washizu, M., Jones, T. B., *J. Electrostat.* 1994, *33*, 187–198.

[45] Watarai, H., Sakamoto, T., Tsukahara, S., *Langmuir* 1997, *13*, 2417–2420.

[46] Ikeda, I., Monjushiro, H., Watarai, H., *Analyst* 2005, *130*, 1340–1342.

[47] Kuokkanen, M. H., *Cent. Eur. J. Phys.* 2010, *8*, 178–183.

[48] Humble, P. H., Kelly, R. T., Woolley, A. T., Tollety, D. H., Lee, M. L., *Anal. Chem.* 2004, *76*, 5641–5648.

[49] Yan, D., Yang, C., Nguyen, N.-T., Huang, X., *Electrophoresis* 2006, *27*, 620–627.

[50] Jones, H. K., Ballou, N. E., *Anal. Chem.* 1990, *62*, 2484–2490.

[51] Petersen, S. L., Ballou, N. E., *Anal. Chem.* 1992, *64*, 1676–1681.

[52] Badal, Y. M., Wong, M., Chiem, N., Salimi-Moosavi, H., Harrison, D. J., *J. Chromatogr. A* 2002, *947*, 277–286.

